Liver-spleen contrast standardization of gadolinium-ethoxybenzyl-diethylenetriamine penta-acetic acid-enhanced magnetic resonance imaging based on cross-calibration

Hiroshige Mori[1]^, Satoru Akimoto[1,2]

[1]Department of Radiology, Japan Community Healthcare Organization Hokkaido Hospital, Hokkaido, Japan; [2]Radiation Room, Japan Community Healthcare Organization Noboribetsu Hospital, Hokkaido, Japan

Contributions: (I) Conception and design: H Mori; (II) Administrative support: S Akimoto; (III) Provision of study materials or patients: Both authors; (IV) Collection and assembly of data: Both authors; (V) Data analysis and interpretation: Both authors; (VI) Manuscript writing: Both authors; (VII) Final approval of manuscript: Both authors.

Correspondence to: Hiroshige Mori, PhD. Department of Radiology, Japan Community Healthcare Organization Hokkaido Hospital, 1-8-3-18 Nakanoshima, Toyohira, Sapporo, Hokkaido 062-8618, Japan. Email: mori-hiroshige@hokkaido.jcho.go.jp.

Background: Liver-spleen contrast in the hepatobiliary phase highly depends on the devices used for liver function tests. This study aimed to develop and validate a method to convert liver-spleen contrast data acquired with another device to reference liver-spleen contrast data, using the regression line of phantom contrasts (i.e., cross-calibration).

Methods: As cohort studies, two-dimensional gradient echo images of T1-weighted fat-suppression in the hepatobiliary phase were retrospectively obtained and analyzed for a total of 126 patients who underwent gadolinium-ethoxybenzyl-diethylenetriamine penta-acetic acid-enhanced magnetic resonance imaging using four different magnetic resonance imaging scanner-coil combinations. The liver-spleen contrast measured from these images was converted into reference liver-spleen contrast using cross-calibration with purified water and gadolinium-ethoxybenzyl-diethylenetriamine penta-acetic acid phantoms of 0.06, 0.14, 0.27, 0.63, 1.37, and 2.82 mM/L. At this point, the error of the regression lines with phantom contrasts was assessed and corrected. Lastly, the liver-spleen and converted liver-spleen contrasts, which are the values before and after cross-calibration respectively, were compared with reference liver-spleen contrast in three cases using different coils and magnetic resonance imaging scanners from a reference device.

Results: Regarding the regression lines with phantom contrasts, the coefficient of determination was 0.99. Although regression lines with phantom contrasts tended to be 0.0105 lower in logarithmic contrasts than those with liver-spleen contrast, no significant difference was observed between the two lines (P=0.0612) by analysis of covariance. In the case of different coils, there was a significant difference between liver-spleen and reference liver-spleen contrasts (P<0.00001), but there was no significant difference between converted liver-spleen and reference liver-spleen contrasts (P=0.492). Moreover, the regression equation between converted liver-spleen and reference liver-spleen contrasts corresponded with an identity line. Likewise, in the two cases of different magnetic resonance imaging scanners, there was a significant difference between liver-spleen and reference liver-spleen contrast (both P<0.00001), but there was no significant difference between converted liver-spleen and reference liver-spleen contrast (P=0.923 and P=0.541).

Conclusions: Cross-calibration using the precision and valid regression lines with phantom contrasts had high accuracy and utility.

Quant Imaging Med Surg 2022;12(12):5343-5357 | https://dx.doi.org/10.21037/qims-22-174

Introduction

In the periodic screening examination for the detection of hepatocellular carcinoma, gadolinium-ethoxybenzyl-diethylenetriamine penta-acetic acid (Gd-EOB-DTPA)-enhanced magnetic resonance imaging (MRI), which includes the assessment of liver function, can provide the benefits of cost savings and convenience to patients with chronic liver diseases (1,2). To assess liver function using Gd-EOB-DTPA-enhanced MRI, the following four approaches have been suggested (2): T_1 or T_2* relaxometry (3), dynamic contrast-enhanced MRI (4), biliary enhancement (5), and liver-spleen contrast (LSC) (6-9). However, it can be difficult to distinguish between normal and Child-Push A using the T_1 or T_2* relaxometry evaluation method (3). In the calibration of signal intensity (SI) data, the hepatobiliary phase images in dynamic contrast-enhanced MRI differ from another phase images, such as the precontrast images, because other sequences are performed during the long wait time between the equilibrium and hepatobiliary phases (10). Additionally, these two methods require dedicated software for calculation or analysis and are costly (2-4). In biliary enhancement, random errors may be a problem when the region of interest (ROI) is too small to measure SI (11,12). On the other hand, the acquisition of LSC is possible by one breath hold in the hepatobiliary phase, and does not require expensive software (2,6). ROIs may be set at an arbitrary placement and adequate size (2,7). Moreover, LSC can be used to separate normal cases from the Grade 1 group of the albumin-bilirubin (ALBI) Grades (13). Therefore, LSC is the simplest and most common technique among these four methods (2).

In pharmacokinetic systems, Gd-EOB-DTPA has specifically taken up normal hepatocytes for bilirubin transport and metabolism through receptors on hepatocyte membranes (6). Gd-EOB-DTPA is also distributed non-specifically to the extracellular fluid (ECF) (14). Therefore, the contrast enhancement effect of Gd-EOB-DTPA is caused not only by hepatocyte uptake but also by an ECF pool (15). Due to the fact that liver enhancement of the ECF can approximate spleen enhancement (14,15), LSC is adopted as the index of hepatic function in Gd-EOB-DTPA-enhanced MRI. While liver function tests through laboratory examination evaluate the entire liver, the LSC can also evaluate zonal and lobar differences of the liver with high-resolution images (16). Moreover, Gd-EOB-DTPA-enhanced MRI can evaluate the future remnant liver functional reserve after hepatectomy by adding the liver volume to the LSC because the volume data can be obtained (15). Moderate correlations have also observed between the LSC and other liver function indexes, such as ALBI score, Child-Push class, and indocyanine green retention rate at 15 min (6,13,15). The LSC levels are also associated with severity of chronic liver diseases (13).

However, LSC is slightly inferior in quantitative value, because the measured SI to calculate LSC is highly dependent on the MRI scanner, acquisition parameters, and scanned body regions or patients (*Figure 1*) (2,7). For example, even if the type of coil is different, the LSC value differs by approximately 30% (7). For LSC, the conversion of SIs into relaxation rates through T_1 relaxation time has been reported (8,9). However, these methods were verified only by a single device, which is MRI scanner-coil combination, from the same manufacturer, and addressing the limitation of LSC dependence on MRI scanners and acquisition parameters was questionable. Although the differences in the contrast among the devices can be minimized by aligning the acquisition parameters with the sensitivity corrections of phased array uniformity enhancement (PURE) (17), this method is not too suitable for the current situation of diverse sequences.

Therefore, to address this problem and as a new way of the standardization of LSC, we invented the conversion of the LSC into reference LSC (rLSC) acquired with another device through regression lines calculated from phantom contrasts (PC). The aim of this work was to assess the accuracy of this cross-calibration conversion technique, regarding the relationship between two different MRI scanner-coil combinations as a pilot study

of standardization. We present the following article in accordance with the STROBE reporting checklist (available at https://qims.amegroups.com/article/view/10.21037/qims-22-174/rc).

Methods

Patients

All patient information were retrospectively collected and anonymized prior to analysis, by adding symbols, such as numbers. This study was conducted in accordance with the Declaration of Helsinki (as revised in 2013). The study design was approved by the ethics review board of the Japan Community Healthcare Organization Hokkaido Hospital (No. 2018-21). Given the retrospective nature of this study, the requirement for written informed consent was waived. We appealed for consent for the secondary use of medical data, by disclosing the research contents on a physical notice board and home page (https://hokkaido.jcho.go.jp/wp-content/uploads/2018/09/NEW2018-21.pdf), as per the provisions of the "Ethical guidelines for medical and health researches involving human subjects" (Ministry of Education, Culture, Sports, Science and Technology and Ministry of Health, Labour, and Welfare bulletin No.3 of 2014).

Images from patients who underwent Gd-EOB-DTPA-enhanced MRI using different MRI scanner-coil combinations from January 4, 2008 to March 31, 2021 were eligible for this study. Images with artifacts and those obtained from patients who had undergone splenectomy were excluded. The collected patient information was classified according to the model of the used MRI scanner. As an index for liver function evaluation, the ALBI score (18) was calculated using the values of the biochemical tests done within two weeks before and after the MRI, as follows:

$$
\begin{aligned}
ALBI\ score = &\ 0.66 \cdot \log_{10}\left(total\ bilirubin\left[\frac{\mu M}{L}\right]\right) \\
&- 0.085 \cdot \left(albumin\left[\frac{g}{L}\right]\right)
\end{aligned}
\tag{1}
$$

Contrast agents

For Gd-EOB-DTPA-enhanced MRI, 0.025 mM/kg body weight of Gd-EOB-DTPA (Primovist 0.25 mM/mL; Bayer Yakuhin Ltd., Osaka, Japan) was intravenously injected, and the images in the hepatobiliary phase were acquired after

60 minutes at which the Gd-EOB-DTPA of the liver ECF space sufficiently washes out and the LSC reaches a state of equilibrium (14).

Twin phantom design

To measure the contrast distribution in the anterior-posterior direction before verifying the cross-calibration, the 2.0 and 5.0 mM/L phantoms were made in 2.0 L PET bottles (10.5 cm × 9.0 cm × 23.0 cm) using reagent grade anhydrous copper (II) sulfate ($CuSO_4$) (Alfa Aesar, Thermo Fisher Scientific, Heysham, United Kingdom). The placement of the 5.0 and 2.0 mM/L $CuSO_4$ phantoms is shown in *Figure 2A,2B*.

For cross-calibration, the 0.06, 0.14, 0.27, 0.63, 1.37, and 2.82 mM/L phantoms of the Gd-EOB-DTPA contrast, referred to the previous research regarding gadolinium-based contrast medium (19), were made in 500-mL PET bottles (5.6 cm × 5.6 cm × 15.0 cm). Additionally, a phantom was made using purified water in a 500-mL PET bottle. The placement of the Gd-EOB-DTPA aqueous solution and purified water phantoms was shown in *Figure 2C*. PC was measured by changing only the molarity of the Gd-EOB-DTPA phantoms.

The T_1 and T_2 values of these phantoms were measured using inversion recovery and spin echo methods, respectively.

Imaging apparatuses and procedures

The device used to acquire rLSC in all examinations was a scanner with a four-channel torso phased array coil (T-PAC) [SIGNA Horizon LX (Echo Speed) 1.5T Ver. 9.1, General Electric Healthcare Japan, Tokyo, Japan]. For the acquisition of converted LSC, the aforementioned device with another body coil (BC) that was built into MRI scanner was used for sample A, and another scanner with a 32-channel sensitivity encoding parallel imaging torso cardiac coil (SENSE-PAC) and a quadrature BC (Q-BC) (Achieva 1.5T A-series R.2.6, Philips Medical Systems Japan, Tokyo, Japan) was used for sample B on another day. The image processing workstation (Advantage Workstation Ver. 4.0, General Electric Healthcare Japan, Tokyo, Japan) and software (Basic Viewing, Philips Medical Systems Japan, Tokyo, Japan) were used to measure the SIs of T-PAC/BC and SENSE-PAC/Q-BC, respectively.

In all phantoms and patients, T_1-weighted transverse images with T-PAC, BC SENSE-PAC, and Q-BC, which
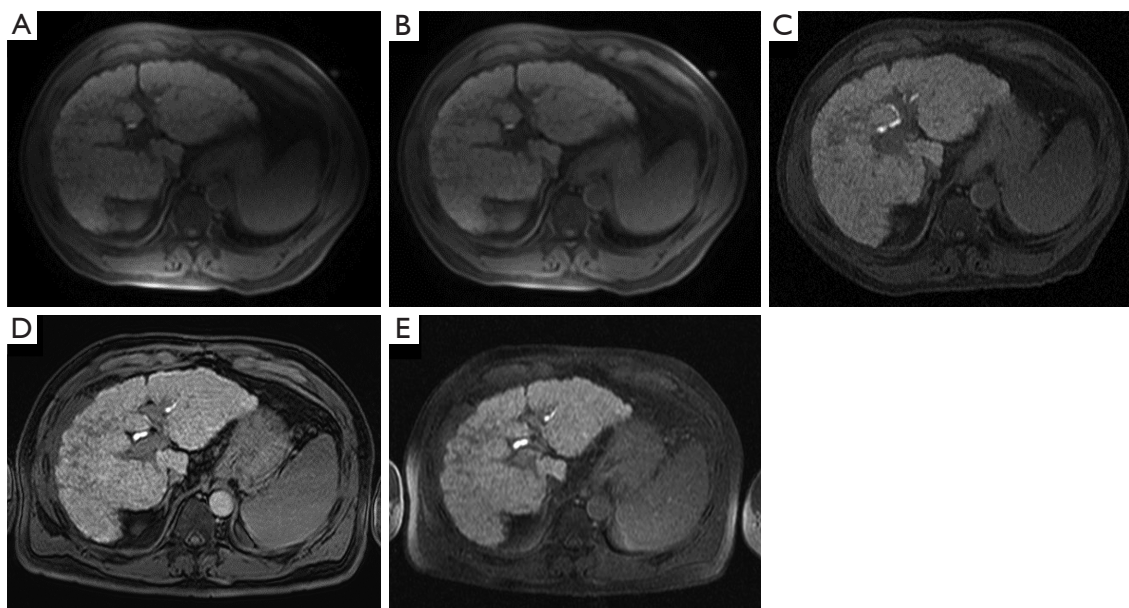
Figure 1 Images in the hepatobiliary phase acquired by various devices and acquisition parameters. Each of the liver-spleen contrast differs. (A) Image before sensitivity correction with the PAC. (B) Image after surface coil intensity correction with the PAC. (C) Image with the built-in body coil. (D) Image after contrast level appearance with the PAC. (E) Image with the built-in quadrature body coil. PAC, phased array coil.

are shown in *Figure 1A,1C-1E*, respectively, were acquired using scan parameters presented in *Table 1*. The slice gap in two-dimensional images was set at ≥20% of the slice thickness to minimize the effect of crosstalk among slices (7). The reduction factor of image-based parallel imaging was 2.0. Surface coil intensity correction (SCIC) was not adopted (*Figure 1A*) because the contrast among organs reduces due to additional smoothing technique (*Figure 1B*) (20). PURE could not be used because it was not built into the scanner used. Contrast level appearance (CLEAR) was applied in sample B (*Figure 1D*).

Image analysis

The ROI size of a rectangle was set to approximately 50 pixels, which is reported to be the minimum number of pixels required to suppress random error (11). The ROI was placed at the location with the smallest standard deviation in order to minimize signal fluctuation (7,11). For measuring the PC, the ROI was set at the center of the phantom (*Figure 2C*). For measuring the LSC, the vasculature and tumor were excluded from the ROI locations (*Figure 2D*). The ROIs were acquired multiple times from five continuous cross sections at the right lobe (12).

On PAC, the SI was the concave distribution in the anterior–posterior direction, which was perpendicular to the anterior and posterior PACs, because the PAC was made by linking the small plural radiofrequency coils on a plane (*Figure 1A*) (21). Furthermore, even if the SCIC was applied, the SI drop remained in the central portion of the images (*Figure 1B*) (21). Therefore, in measuring the contrasts using T-PAC, two ROIs of the liver and spleen were placed at the same distance from the PACs in order to keep the same condition of the SI drop between these two ROIs (*Figure 2C,2D*). For measuring the LSC, the ROI in the liver was set using the smallest standard deviation, followed by placement of the ROI in the spleen at the same height as that of the liver (*Figure 2D*) (7). However, when using the built-in BC, aligning the heights of these two ROIs is not needed, because the BC had uniform sensitivity in effective imaging regions (*Figure 1C,1E*). In the SENSE-PAC with CLEAR, these ROIs are not aligned (*Figure 1D*).

Contrasts were calculated using the following Michelson contrast formulas (13,22):

$$Contrast = \frac{SI_1 - SI_2}{SI_1 + SI_2} \qquad [2]$$
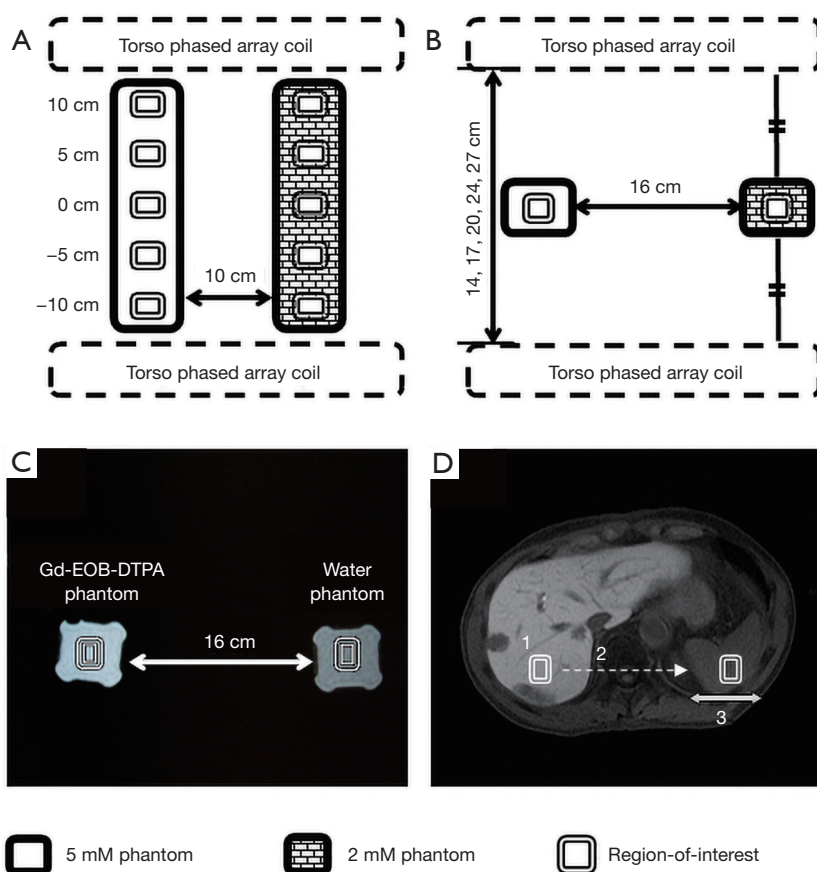
and

Figure 2 Geometry of phantoms and/or ROIs for contrast measurements. The height of two region-of-interests is aligned in using PACs. (A) Distributions in the anterior-posterior direction. (B) Influence of the interval between the confronting PACs on the anterior-posterior direction. (C) Phantom contrasts. Gd-EOB-DTPA and water phantoms are placed at 5 cm on a bed. (D) Steps for liver-spleen contrast measurements. 1, locate the area in the liver ROI where the standard deviation is lowest in the right hepatic lobe; 2, look for the location within the spleen that is level with the liver ROI; and 3, place the spleen ROI in the location where the standard deviation is lowest in the area selected in step 2. ROIs, region-of-interests; PACs, phased array coils; Gd-EOB-DTPA, Gadolinium-ethoxybenzyl-diethylenetriamine penta-acetic acid.

$$-1 \leq Contrast \leq 1 \tag{3}$$

In the PCs, the SI_1 and SI_2 represented the phantom SIs on the liver and spleen sides, respectively. For the LSC, the SI_1 and SI_2 represented the SIs of the liver and spleen, respectively. The measured value was the average of the contrast values of five images.

The Michelson contrast is an index that normalizes the difference between light and dark signals with the average value of both and is used in optical systems, such as the theory of signal processing (22,23). When an object on MRI has a wide dynamic range, the Michelson contrast, compared with the contrast ratio (6,16), is said to closely approximate the actual evaluation, because the object on contrast ratio, which

is the ratio of two SIs, is not assumed to be a logarithmic response (22,23). In this study, the Michelson contrast was selected with the intent to exclude the liver enhancement effect of ECF. For the comparison with previous studies using other contrast formulas, the conversion formula from contrast ratio (C_r) and Weber contrast (C_W) (15) to Michelson contrast (C_M) is shown below:

$$C_M = \frac{C_r - 1}{C_r + 1} = \frac{C_W}{C_W + 2} \tag{4}$$

Verification of the setting method of two ROIs

To verify the method of aligning the height of the two

Table 1 Acquisition parameters

Device scan parameter	SIGNA Horizon LX	Achieva A-series	
		Phased array coil	Body coil
Dimension	2	3	2
Sequence	Fast SPGR	FFE, e-THRIVE	FFE of multislice
Fat suppression	CHESS	SPAIR	ProSet
Echo time (ms)	1.3	2.3	5.1
Repetition time (ms)	148	4.6	126
Flip angle (°)	70	10	80
Number of excitations	1	1	1
k-space trajectory	Sequential	Linear	Linear
Band width (Hz/pixel)	325.5	360.8	313.8
Field of view (mm)	430	370	420
Matrix (frequency × phase)	256×160	240×153	256×160
Scan percentage (%)	100	79.8	62.5
Phase field of view (%)	75	80	100
Slice thickness (mm)	6.5	4.0	6.5
Slice gap (mm)	3.5	0	3.5
Slice scan order	Slice number	–	Interleaved
Slice number	20	40	7
Respiration	Breath hold	Breath hold	Breath hold
Scan time (s)	10.0	14.3	20.7

SPGR, spoiled gradient recalled acquisition of steady state; FFE, fast field echo; e-THRIVE, enhanced-T_1 high resolution isotropic volume excitation; CHESS, chemical shift saturation; SPAIR, spectral attenuated with inversion recovery; ProSet, principle of selective excitation technique.

ROIs adopted in this study, the phantoms of $CuSO_4$ aqueous solution were perpendicularly placed, and the PC distribution in the anterior-posterior direction was measured at 0, 5, and 10 cm away from the center between the anterior and posterior T-PACs (*Figure 2A*). The measurement values were represented by the ratio to the center (0 cm).

In addition, the influence of the interval between confronting PACs on contrasts (21) was examined with the aim of grasping the influence of body thickness on contrasts. The phantoms of $CuSO_4$ aqueous solution were set on the center between the anterior and posterior T-PACs, and the PC was measured at intervals of 14, 17, 20, 24, and 27 cm (*Figure 2B*). The measurement values were represented by the ratio to the value measured at 20 cm.

Acquisition of regression lines with PC

Because the relationship between the molarity and T_1-weighted Gd contrast becomes a sigmoid curve at low and medium concentrations (19), it is assumed that this relationship can be approximated to a straight line by logarithmically converting PC. Therefore, the relationship between the PC of the converted device and the PC of the reference device (i.e., rPC) was formulated using the following regression line:

$$\log_{10} rPC = a_0 \cdot \log_{10} PC + b_0 \tag{5}$$

where a_0 and b_0 were the slope and intercept, respectively.

However, because the Michelson contrast had a negative value in Eq. [3], the antilogarithm in Eq. [5] was aligned
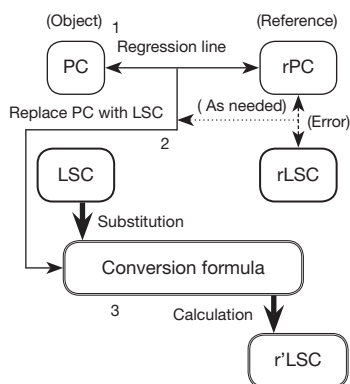
Figure 3 Flowchart of cross-calibration. The thick arrows represent the procedure of cross-calibration. 1, create the regression line of PC with a reference device (Eq. [6]); 2, replace the PC with the LSC in the above regression line. If there is error between the PC and LSC, add a correction (Eq. [8]); and 3, substitute the values of the LSC into the conversion Eq. [9]. rPC, PC of a reference device; rLSC, LSC of a reference device; r'LSC, LSC converted into the rLSC by cross-calibration. PC, phantom contrast; LSC, liver-spleen contrast.

to a positive value by adding 1, as shown in the following linear equation:

$$\log_{10}\left(1+rPC\right) = a_p \cdot \log_{10}\left(1+PC\right) + b_p \qquad [6]$$

and

$$0 < 1+PC < 2 \qquad [7]$$

where a_p and b_p were the slope and intercept, respectively.

To obtain the regression line (i.e., Eq. [6]), PCs were measured at multiple molarities of the Gd-EOB-DTPA phantoms. In sample A, in which only the coil differed from the reference device, the regression line was acquired from T-PAC and BC. In sample B, in which the acquisition parameter and MRI scanner differed from the reference device, the regression line was acquired from T-PAC and SENSE-PAC/Q-BC.

Cross-calibration of the LSC

The PC of Eq. [6] was replaced by LSC, as follows:

$$\log_{10}\left(1+r'LSC\right) = a_p \cdot \log_{10}\left(1+LSC\right) + b_p + E \qquad [8]$$

where E was the system error between PC and LSC. The r'LSC was the LSC converted into the rLSC by cross-

calibration. Eq. [8] was transformed, as follows:

$$r'LSC = 10^{a_p \cdot \log_{10}\left(1+LSC\right)+b_p+E} - 1 \qquad [9]$$

First, to obtain the E of Eq. [8], the regression line of the LSC between T-PAC and BC was acquired from sample A and was compared with the regression line of the PC between T-PAC and BC. Second, the conversion formula (i.e., Eq. [9]) was calculated from the regression line and E. Thirdly, the LSCs of BC, SENSE-PAC, and Q-BC were substituted for the conversion formula, and cross-calibration from LSC to r'LSC was performed in samples A and B. Lastly, each LSC and r'LSC was compared with the rLSC to examine the effect and accuracy of cross-calibration, respectively.

In creating the cross-calibration mentioned above, we referred to the method of standardizing the heart-to-mediastinum ratio in myocardial sympathetic scintigraphy using ^{123}I-metaiodobenzylguanidine (24). The process of cross-calibration is shown in *Figure 3*.

Statistical analysis

For the comparison between subject groups, a student's *t*-test was performed assuming equal various between two samples. For the comparison of SI or contrast distribution between T-PAC and BC, analysis of variance (ANOVA) in a two-way layout was performed. The regression line was calculated by linear regression analysis. After carrying out the test of no correlation, Pearson's correlation coefficient (R), the coefficient of determination (R^2), and standard error (SE) were also calculated on all regression analyses. In sample A, the LSC and r'LSC were compared with rLSC using paired *t*-test and regression analysis. In sample B, LSC and r'LSC were compared with rLSC using analysis of covariance (ANCOVA) with the ALBI scores. ANCOVA was performed to remove any confounding effect of the patient's liver function; this was because the LSC or r'LSC by SENSE-PAC and Q-BC was not acquired on the same day as the rLSC by T-PAC was acquired. After testing the parallelism of the regression lines between groups and the significance of regression (slope ≠ 0), the difference of the intercepts between groups was tested. ANCOVA was also performed for the comparison of the regression lines of PC and LSC.

In all statistical tests, a two-sided probability (P) value of less than 0.05 was considered to indicate a statistical significance. The 95% confidence interval (CI) was calculated as the interval estimation. All statistical analyses
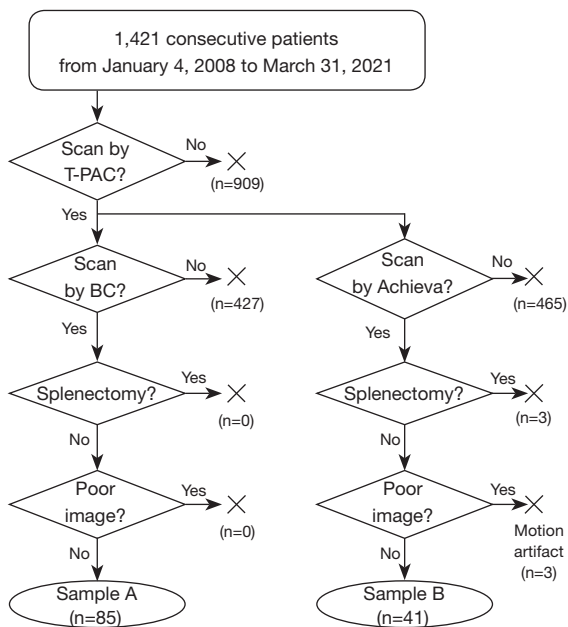
5350

Mori et al. Cross-calibration of liver-spleen contrasts in Gd-EOB MRI

Figure 4 Flow diagram to sort out enrollment subjects. T-PAC, torso phased array coil; BC, body coil; ×, exclusion; n, number of patients.

were carried out using the Analysis ToolPak in Excel Add-ins (Microsoft Excel 2010 SP2, Microsoft Corporation, Washington, USA).

Results

Subject groups

After excluding unsuitable cases based on the criteria mentioned above from 1,421 patients who underwent Gd-EOB-DTPA-enhanced MRI, 126 participants (77 men and 49 women) remained. The final numbers of sample A and B were 85 and 41 patients, respectively. The selection of this study population is presented in *Figure 4*. The patient details and clinical features are shown in *Table 2*. There was no significant difference in the factors that influenced the images between sample A and B (P>0.05).

Relaxation times of phantoms

The 2.0 and 5.0 mM/L phantoms of $CuSO_4$ aqueous solution had T_1 values of 570 and 331 ms, respectively, and T_2 values of 561 and 197 ms, respectively.

The 0.06, 0.14, 0.27, 0.63, 1.37, and 2.82 mM/L

phantoms of the Gd-EOB-DTPA aqueous solution had T_1 values of 3,400, 1,900, 1,500, 960, 460, and 260 ms, respectively, and T_2 values of 1,800, 1,200, 610, 420, 170, and 91 ms, respectively.

Verification of the setting method of two ROIs

The distributions of SI and contrast in the anterior–posterior direction are shown in *Figure 5A,5B*, respectively. In BC, the distributions of SI and contrast were almost constant, regardless of ROI locations. In T-PAC, the SI increased as it approached the PACs, and the SI that was near the PAC was about twice of that in the center. However, by aligning the height of two ROIs in the anterior–posterior direction, the contrast variation was suppressed to about 10%.

The influences of the interval between confronting PACs on SI and contrast are shown in *Figure 5C,5D*, respectively. In BC, the SI and contrast were constant regardless of the interval between confronting PACs. In T-PAC, the SI decreased as the interval between confronting PACs increased, and the SI in the interval of 27 cm was half of that in the interval of 14 cm. However, the contrast was constant at an interval of ≥17 cm, which largely covered the body thickness of the subjects measured in this study (*Table 2*). Even at an interval of 14 cm, the difference in the contrast with BC was about 10%.

Acquisition of regression lines with PC

The relationship between the PC of BC, SENSE-PAC, or Q-BC and the rPC of T-PAC is shown in *Figure 6A*. In the PC of BC, the regression line with rPC was as follows:

$$\log_{10}\left(1+rPC\right)=1.242\bullet\log_{10}\left(1+PC\right)-0.081 \qquad [10]$$

In the PC of SENSE-PAC, the regression line with rPC was as follows:

$$\log_{10}\left(1+rPC\right)=1.213\bullet\log_{10}\left(1+PC\right)-0.096 \qquad [11]$$

In the PC of Q-BC, the regression line with rPC was as follows:

$$\log_{10}\left(1+rPC\right)=1.180\bullet\log_{10}\left(1+PC\right)-0.107 \qquad [12]$$

The R and R^2 values of these three regression lines were both 0.99. Moreover, their SEs were both less than 0.005.

Table 2 Patient background

Item	Sample A	Sample B	P value
Sample			
Size	85	41	
Sex (male/female) (n)	56/29	21/20	
Age (years)	68.7±16.2 (29 to 89)	68.4±8.7 (52 to 86)	0.511
Physique			
Body weight (kg)	63.4±9.1 (46.0 to 104.0)	64.4±8.5 (50.0 to 85.0)	0.576
Body thickness (cm)	22.2±2.2 (16.0 to 29.3)	22.4±2.1 (16.7 to 26.4)	0.650
Body width (cm)	30.6±2.2 (24.6 to 36.8)	30.6±2.3 (25.8 to 35.0)	0.878
Liver disease (n)			
Chronic viral hepatitis (type B and/or C)	16	11	
Liver cirrhosis (hepatitis B and/or C)	35	19	
Alcoholic liver disease	13	7	
Nonalcoholic fatty liver disease	4	2	
Primary biliary cholangitis	1	0	
Normality	16	2	
Mass (HCC/metastasis) (n)	50/6	32/0	
Liver function test			
ALBI score	−2.46±0.57 (−3.30 to −0.92)	−2.55±0.44 (−3.41 to −1.43)	0.353
ALBI grade (Grade 1/Grade 2/Grade 3) (n)	43/35/7	20/21/0	
Classic liver function data			
Albumin (g/dL)	3.78±0.60 (2.40 to 4.80)	3.85±0.51 (2.60 to 4.80)	0.542
Total bilirubin (mg/dL)	0.95±0.64 (0.20 to 3.90)	0.78±0.34 (0.30 to 2.00)	0.114
Direct bilirubin (mg/dL)	0.40±0.48 (0.06 to 3.22)	0.35±0.45 (0.07 to 3.00)	0.575

All data except those indicated as n represent mean ± standard deviation (minimum to maximum). P, probability; n, number of patients; HCC, hepatocellular carcinoma; ALBI, albumin-bilirubin.

Cross-calibration of the LSC

The relationship between the LSC of BC and the rLSC of T-PAC is shown in *Figure 6B*. The PCs of up to 1.37 mM/L were included in the range of the LSC. On ANCOVA, the PC tended to be 0.0105 lower than the LSC in the logarithmic contrasts, but no statistically significant difference in the LSC was detected (P=0.0612). Therefore, the E of Eq. [8] was defined as 0.0105.

In the case sample A, the conversion formula was as follows:

$$r'LSC = 10^{1.242 \cdot \log_{10}(1+LSC) - 0.0711} - 1 \qquad [13]$$

On paired *t*-test, the rLSC significantly differed from the LSC (P<0.00001, 95% CI: 0.0824–0.151) but not from the r'LSC (P=0.492). The effect of cross-calibration in sample A is shown in *Figure 7*. The regression equation between r'LSC and rLSC after cross-calibration was as follows:

$$rLSC = 0.969 \cdot r'LSC + 0.0107 \qquad [14]$$

The regression coefficient between r'LSC and rLSC was about 1.0 (P<0.00001, 95% CI: 0.827–1.110). The intercept was not statistically significant (P=0.461). Therefore, this regression equation corresponded with the line of identity
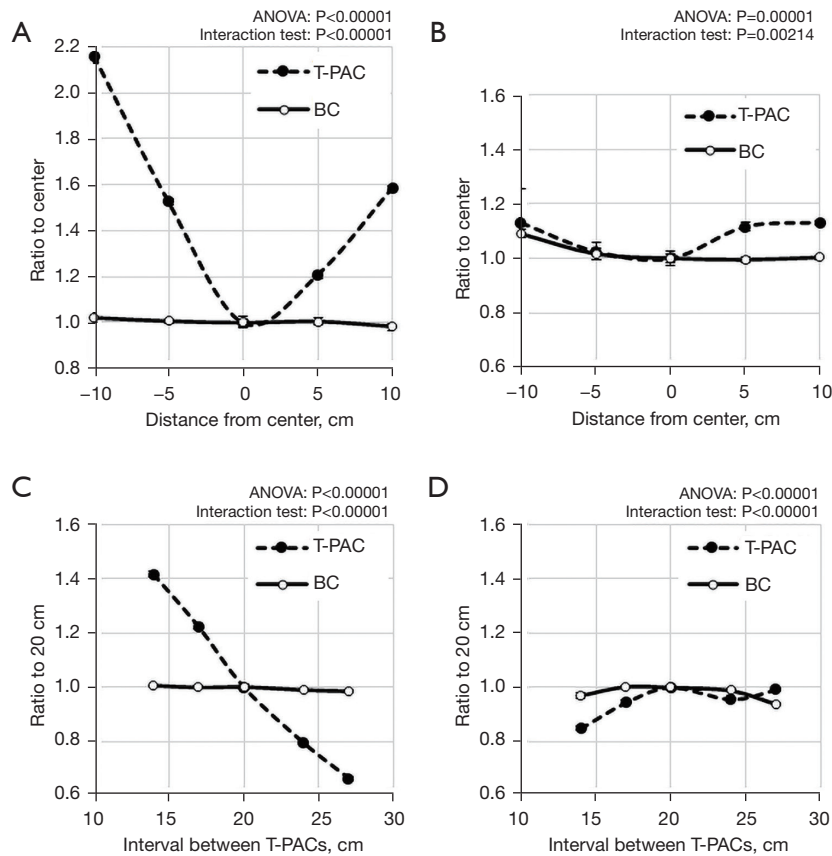
5352

Mori et al. Cross-calibration of liver-spleen contrasts in Gd-EOB MRI

Figure 5 Comparison of the distribution between T-PAC and body coil (BC). On T-PAC, although SI fluctuates, PC is stable like BC. (A) SI distribution in the anterior–posterior direction in a 5.0-mM/L CuSO$_4$ phantom. (B) PC distribution in the anterior-posterior direction. (C) Relationship between the interval of T-PACs and the SI in a 5.0-mM/L CuSO$_4$ phantom. (D) Relationship between the interval of T-PACs and the PC. ANOVA, analysis of variance; P, probability; T-PAC, torso phased array coil; SI, signal intensity; PC, phantom contrast.
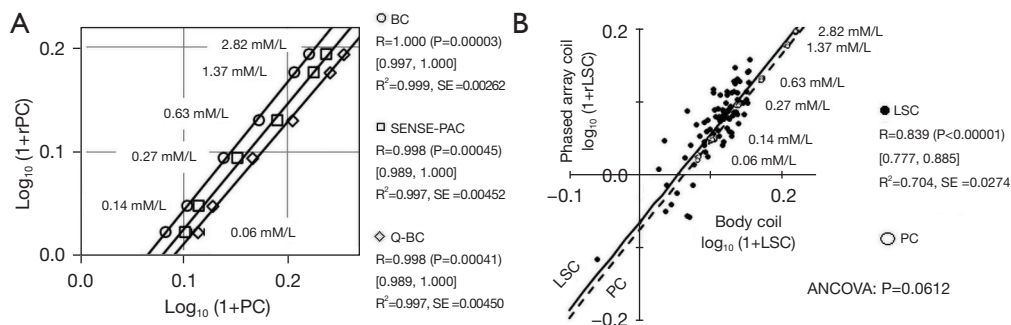
Figure 6 Regression lines of PC and LSC. The values in the figures represent the molarity (mM/L) of the Gadolinium-ethoxybenzyl-diethylenetriamine penta-acetic acid phantoms. All regression lines have strong linearity with a R of ≥0.8 and have strong reliability with a R^2 of ≥0.7. The 95% confidence interval is presented as numbers in square brackets. (A) Relationships between PC and the rPC. (B) Relationship between the LSC of BC and the rLSC. Parallelism of regression lines (P=0.659); significance of regression (P<0.00001); 95% confidence interval of PC and LSC [(0.0619, 0.0804) and (0.0765, 0.0870)]. SENSE-PAC, sensitivity encoding parallel imaging torso cardiac coil; Q-BC, quadrature body coil; SE, standard error; ANCOVA, analysis of covariance; P, probability; PC, phantom contrast; LSC, liver-spleen contrast; BC, body coil; rLSC, LSC of a reference device; rPC, PC of a reference device; R, correlation coefficient; R^2, coefficient of determination.
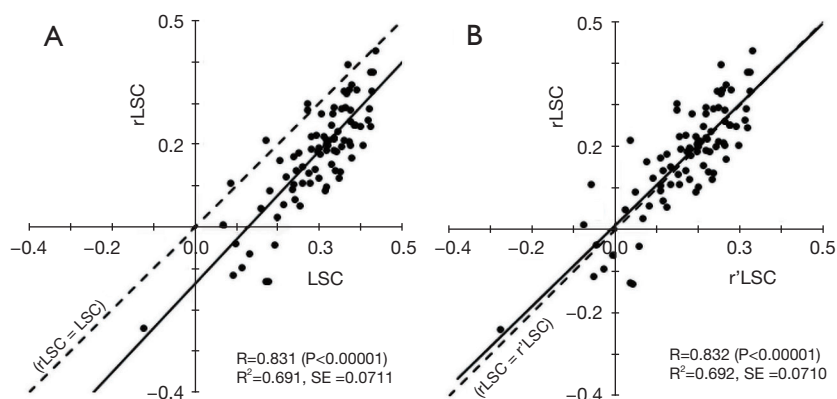
Figure 7 Effect of cross-calibration in the case in which only the coil differed (sample A). The dotted lines represent the lines of identity. The difference between the LSC and the rLSC is removed by cross-calibration. (A) Comparison of the LSC and rLSC before cross-calibration. (B) Comparison of the LSC converted into the rLSC (r'LSC) and rLSC after cross-calibration. LSC, liver-spleen contrast; rLSC, LSC of a reference device; R, correlation coefficient; R^2, coefficient of determination; SE, standard error.

(*Figure 7B*). Before and after cross-calibration, the SEs were both 0.071 and did not change.

The effect of cross-calibration in sample B is shown in *Figure 8*. In SENSE-PAC, the conversion formula was as follows:

$$r'LSC = 10^{1.213 \cdot \log_{10}(1+LSC)-0.0856} - 1 \qquad [15]$$

The rLSC significantly differed from the LSC (P<0.00001, 95% CI: 0.138–0.207) (*Figure 8A*) but not from the r'LSC (P=0.923) (*Figure 8B*). In Q-BC, the conversion formula was as follows:

$$r'LSC = 10^{1.180 \cdot \log_{10}(1+LSC)-0.0969} - 1 \qquad [16]$$

The rLSC significantly differed from the LSC (P<0.00001, 95% CI: 0.159–0.234) (*Figure 8C*) but not from the r'LSC (P=0.541) (*Figure 8D*). The 95% CI values of the LSC, r'LSC, and rLSC were stable within an interval of 0.05, which did not change before and after cross-calibration.

Discussion

Although a built-in BC that has a uniform SI distribution is an ideal coil to quantitatively measure contrasts, Gd-EOB-DTPA-enhanced MRI is generally performed with PACs to acquire images of high sensitivity and resolution (20). PACs have a concave distribution of SI (21). Therefore, it is necessary to smooth this distribution by an image-based correction technique (e.g., SCIC or homogeneity correction), which adjusts the SIs by predetermined coefficients, or a calibration-based correction technique (e.g., PURE or CLEAR), which uses the reference images of the built-in BC (20,21). However, it had been pointed out that the images rendered by these correction methods cannot be used for quantitative evaluation using contrasts, because these techniques lower the LSC and cannot recover the contrast among organs (20). Our study indicated that the measurement method of aligning the height of two ROIs on an anterior-posterior direction can suppress the variation of contrasts by 10% without correcting the SIs. In addition, within the expected range of body thickness, measurement of the contrasts in uniform distribution was possible, regardless of the positions of the PACs on the anterior-posterior direction (21). The method used in this study entailed acquisition of images before the postprocessing for correction. However, the method of aligning two ROIs can largely contribute to the quantitative measurement of the LSC when correction techniques with a phase image or a B1 map were not built into using MRI scanners. In future, MultiTransmit system should be used, because the MultiTransmit parallel radio frequency transmission technology can improve image nonuniformity and has high contrast, compared with body tuned CLEAR (25).

In this study, the linear model obtained by the logarithmic transformation of the contrast values was proposed to represent the relationship of contrasts between two different devices. In PC, both regression lines indicated strong linearity and high reliability. In the LSC, the relationship
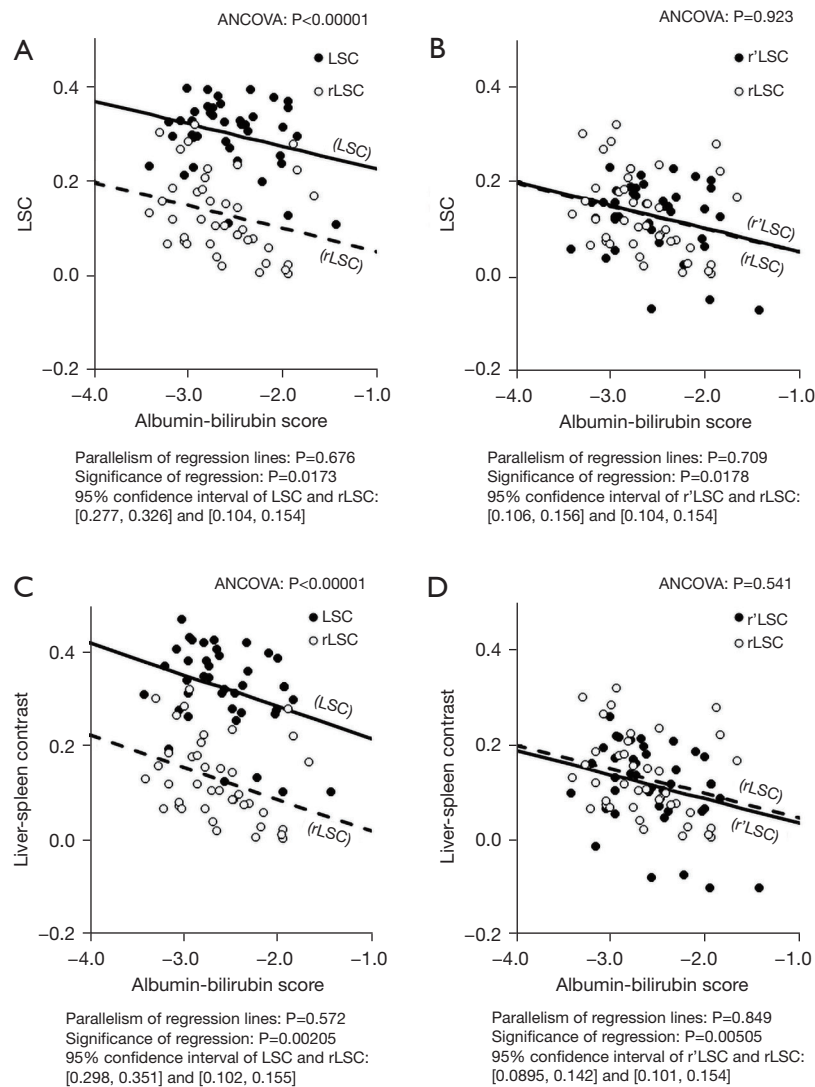
5354

Mori et al. Cross-calibration of liver-spleen contrasts in Gd-EOB MRI

Figure 8 Effect of cross-calibration in the case in which the acquisition parameter and MRI scanner differed (sample B). The difference between the LSC and the rLSC is removed by cross-calibration. ANCOVA is performed using albumin–bilirubin scores. (A) Comparison of the LSC and rLSC before cross-calibration in SENSE-PAC. (B) Comparison of the r'LSC and rLSC after cross-calibration in SENSE-PAC. (C) Comparison of the LSC and rLSC before cross-calibration in Q-BC. (D) Comparison of the r'LSC and rLSC after cross-calibration in Q-BC. LSC, liver-spleen contrast; rLSC, LSC of a reference device; ANCOVA, Analysis of covariance; SENSE-PAC, sensitivity encoding parallel imaging torso cardiac coil; r'LSC, LSC converted into the rLSC; Q-BC, quadrature body coil; P, probability.

between T-PAC and BC showed the same characteristics as that in PC. Therefore, this linear model has validity at a Gd-EOB-DTPA concentration range of up to 2.82 mM/L. For the Gd-EOB-DTPA phantoms, the expected range in the LSC was covered by a concentration range of 0.14 to 1.37 mM/L, except the negative range of the LSC. Additionally, the reference concentrations that simulate normal liver, liver cirrhosis, and tumor were

reported to be 0.63, 0.42, and 0.15 mM/L, respectively (26). Accordingly, the line-up of Gd-EOB-DTPA phantoms corresponded to the variations in the LSC and was valid. There was no significant difference between PC and LSC, and the SE values of PC were small. Therefore, as an alternative to the LSC, the phantoms in this study had sufficient accuracy and precision. In the relationship between T-PAC and BC, the regression line with these phantoms was

almost identical with the equation of the LSC. Therefore, the regression lines obtained from PCs sufficiently reflected the relationship of the LSCs obtained by different devices.

The conversion formulas based on the regression lines of PC had no error in the two cases of different MRI scanner-coil combinations. In terms of system errors, there was no significant difference between r'LSC and rLSC. For random errors, there was no change in the SE or 95% CI values before and after conversion. These results supported the high accuracy and precision of this conversion formula. This conversion formula can correct the system errors of the phantoms. In addition, even if the acquisition parameters of the MRI scanners changed before and after conversion, there was no significant difference between the r'LSCs of SENSE-PAC/Q-BC and the rLSC of T-PAC. Therefore, cross-calibration had high accuracy and utility.

Our study had the limitation of using the unconsidered phantoms about human equivalent electrical conductivity. The phantoms for dilution with purified water had higher T_2 values, compared with that of abdominal living tissues (27). However, the effects of high T_2 values appear to be limited because Gd-EOB-DTPA-enhanced MRI is acquired by minimum echo and repetition times (26). In fact, the difference between PC and the LSC did not significantly differ. If high accuracy of the phantoms is required, the high T_2 values could be improved by dilution with normal saline at 0.9 w/v% (28) and the size of phantoms had better be about a human body to heighten uniformity. Another limitation of our study was that the only three cases of different MRI scanner-coil combinations were compared. Nevertheless, as a pilot study, our findings sufficiently provided clear evidence that our method of cross-calibration of the LSC had high accuracy and universality. Future multicenter studies on cross-calibration are needed to standardize the LSC if the LSC becomes an almost complete substitute for traditional liver function indices with sufficient evidence.

Conclusions

We proposed a method of converting the LSC to rLSC acquired by another device using conversion formulas obtained from PC. Cross-calibration using the regression lines of PC had high accuracy and utility and is sure to contribute to the standardization of the LSC.

Acknowledgments

Footnote

Ethical Statement: The authors are accountable for all aspects of the work in ensuring that questions related to the accuracy or integrity of any part of the work are appropriately investigated and resolved. The study was conducted in accordance with the Declaration of Helsinki (as revised in 2013). The study was approved by the ethics review board of the Japan Community Healthcare Organization Hokkaido Hospital (Research Reference No. 2018-21). Written individual consent for this retrospective analysis was waived.

References

1. Xie S, Liu C, Yu Z, Ren T, Hou J, Chen L, Huang L, Cheng Y, Ji Q, Yin J, Zhang L, Shen W. One-stop-shop preoperative evaluation for living liver donors with gadoxetic acid disodium-enhanced magnetic resonance imaging: efficiency and additional benefit. Clin Transplant 2015;29:1164-72.

2. Bae KE, Kim SY, Lee SS, Kim KW, Won HJ, Shin YM, Kim PN, Lee MG. Assessment of hepatic function with Gd-EOB-DTPA-enhanced hepatic MRI. Dig Dis 2012;30:617-22.

3. Katsube T, Okada M, Kumano S, Hori M, Imaoka I, Ishii K, Kudo M, Kitagaki H, Murakami T. Estimation of liver function using T1 mapping on Gd-EOB-DTPA-enhanced magnetic resonance imaging. Invest Radiol

2011;46:277-83.

4. Nilsson H, Blomqvist L, Douglas L, Nordell A, Jonas E. Assessment of liver function in primary biliary cirrhosis using Gd-EOB-DTPA-enhanced liver MRI. HPB (Oxford) 2010;12:567-76.

5. Takao H, Akai H, Tajima T, Kiryu S, Watanabe Y, Imamura H, Akahane M, Yoshioka N, Kokudo N, Ohtomo K. MR imaging of the biliary tract with Gd-EOB-DTPA: effect of liver function on signal intensity. Eur J Radiol 2011;77:325-9.

6. Motosugi U, Ichikawa T, Sou H, Sano K, Tominaga L, Kitamura T, Araki T. Liver parenchymal enhancement of hepatocyte-phase images in Gd-EOB-DTPA-enhanced MR imaging: which biological markers of the liver function affect the enhancement? J Magn Reson Imaging 2009;30:1042-6.

7. Mori H, Furuya K, Akimoto S, Ajioka R, Emoto T. Examination of the means of measuring liver function in the hepatobiliary phase. Nihon Hoshasen Gijutsu Gakkai Zasshi 2009;65:1502-11.

8. Norén B, Forsgren MF, Dahlqvist Leinhard O, Dahlström N, Kihlberg J, Romu T, Kechagias S, Almer S, Smedby Ö, Lundberg P. Separation of advanced from mild hepatic fibrosis by quantification of the hepatobiliary uptake of Gd-EOB-DTPA. Eur Radiol 2013;23:174-81.

9. Norén B, Dahlström N, Forsgren MF, Dahlqvist Leinhard O, Kechagias S, Almer S, Wirell S, Smedby Ö, Lundberg P. Visual assessment of biliary excretion of Gd-EOB-DTPA in patients with suspected diffuse liver disease - A biopsy-verified prospective study. Eur J Radiol Open 2015;2:19-25.

10. Onoda M, Hyodo T, Murakami T, Okada M, Uto T, Hori M, Miyati T. Optimizing signal intensity correction during evaluation of hepatic parenchymal enhancement on gadoxetate disodium-enhanced MRI: comparison of three methods. Eur J Radiol 2015;84:339-45.

11. Ogura A, Miyati T, Kobayashi M, Imai H, Shimizu K, Tsuchihashi T, Doi T, Machida Y. Method of SNR determination using clinical images. Nihon Hoshasen Gijutsu Gakkai Zasshi 2007;63:1099-104.

12. Tokorodani R, Kume T, Daikoku K, Oka M. Evaluation of the Validity of ROI Setting in CEI Used for the Assessment of Liver. Nihon Hoshasen Gijutsu Gakkai Zasshi 2022;78:44-52.

13. Mori H, Machimura H, Iwaya A, Baba M, Furuya K. Comparison of liver scintigraphy and the liver-spleen contrast in Gd-EOB-DTPA-enhanced MRI on liver function tests. Sci Rep 2021;11:22472.

14. Dahlqvist Leinhard O, Dahlström N, Kihlberg J, Sandström P, Brismar TB, Smedby O, Lundberg P. Quantifying differences in hepatic uptake of the liver specific contrast agents Gd-EOB-DTPA and Gd-BOPTA: a pilot study. Eur Radiol 2012;22:642-53.

15. Yamada A, Hara T, Li F, Fujinaga Y, Ueda K, Kadoya M, Doi K. Quantitative evaluation of liver function with use of gadoxetate disodium-enhanced MR imaging. Radiology 2011;260:727-33.

16. Okubo H, Mogami M, Ozaki Y, Igusa Y, Aoyama T, Amano M, Kokubu S, Miyazaki A, Watanabe S. Liver function test by gadolinium-ethoxybenzyl-diethylenetriamine pentaacetic acid-enhanced magnetic resonance imaging with consideration of intrahepatic regional differences. Hepatogastroenterology 2013;60:1547-51.

17. Naka T, Takahashi M, Takeda K, Igarashi T, Hondera T. Optimization of T1-weighted Imaging Parameters in MR Carotid Plaque Imaging: Influence for the Quantitative Evaluation among Different MRI Scanner Types. Nihon Hoshasen Gijutsu Gakkai Zasshi 2017;73:104-11.

18. Hiraoka A, Michitaka K, Kumada T, Izumi N, Kadoya M, Kokudo N, Kubo S, Matsuyama Y, Nakashima O, Sakamoto M, Takayama T, Kokudo T, Kashiwabara K, Kudo M. Validation and Potential of Albumin-Bilirubin Grade and Prognostication in a Nationwide Survey of 46,681 Hepatocellular Carcinoma Patients in Japan: The Need for a More Detailed Evaluation of Hepatic Function. Liver Cancer 2017;6:325-36.

19. Kumashiro M, Dohke M, Nakada K. Difference of T1-weighted contrast among various pulse sequences: basic study by using a phantom containing Gd-DTPA solutions. Jpn J Magn Reson Med (JJMRM) 1999;19:528-38.

20. Ogasawara G, Inoue Y, Matsunaga K, Fujii K, Hata H, Takato Y. Image Non-Uniformity Correction for 3-T Gd-EOB-DTPA-Enhanced MR Imaging of the Liver. Magn Reson Med Sci 2017;16:115-22.

21. Kimura T, Tahara D, Iiduka A, Taniguchi Y, Ishikuro A, Hongo T, Inoue H, Ogura A. Examination of measurement and its method of compensation of the sensitivity distribution using phased array coil for body scan. Nihon Hoshasen Gijutsu Gakkai Zasshi 2003;59:1164-73.

22. Michelson AA. Studies in optics. Chicago: Chicago Press; 1927.

23. Peli E. Contrast in complex images. J Opt Soc Am A 1990;7:2032-40.

24. Nakajima K, Okuda K, Matsuo S, Yoshita M, Taki J, Yamada M, Kinuya S. Standardization of metaiodobenzylguanidine heart to mediastinum ratio using

a calibration phantom: effects of correction on normal databases and a multicentre study. Eur J Nucl Med Mol Imaging 2012;39:113-9.

25. Shibukawa S, Horie T, Nishio H, Muro I. Basic examination of uniformity of image and contrast of multi-transmit system. Nihon Hoshasen Gijutsu Gakkai Zasshi 2011;67:1192-9.

26. Oura D, Abe K, Nambu T, Kondo Y. Basic evaluation of the optimal flip angle for hepatocyte phase with gadolinium ethoxybenzyl diethylenetriamine pantaacetic acid: selection of the optimal flip angle by the imaging findings. Nihon Hoshasen Gijutsu Gakkai Zasshi

2013;69:1394-404.

27. de Bazelaire CM, Duhamel GD, Rofsky NM, Alsop DC. MR imaging relaxation times of abdominal and pelvic tissues measured in vivo at 3.0 T: preliminary results. Radiology 2004;230:652-9.

28. Murakami K, Yoshida K, Kakuba K, Yanagimoto S. Contrast-to-noise ratio for liver parenchyma of the large arterial blood maximum density of Gd-EOB-DTPA and Gd-DTPA in first pass dynamic study (3D-FSPGR technique). Nihon Hoshasen Gijutsu Gakkai Zasshi 2009;65:301-5.